Available online at www.sciencedirect.com
ScienceDirect
Journal of the European Ceramic Society 26 (2006) 3499–3507
www.elsevier.com/locate/jeurceramsoc

Synthesis of ultra fine particles by plasma transferred arc: Influence of anode material on particle properties

C. Chazelas, J.F. Coudert, J. Jarrige *, P. Fauchais

SPCTS, CNRS, UMR 6638, University of Science and Technology of Limoges, 123 Avenue Albert Thomas, 87060 Limoges cedex, France

Received 4 October 2005; received in revised form 19 January 2006; accepted 22 January 2006
Available online 9 March 2006

Abstract

There is a great deal of interest today in the special properties of nanoparticles and their potential applications. Gas-phase process, although having some drawbacks, has the largest control possibilities and is therefore the method chosen here. The size of the primary particles depends on the temperature/time history and material properties. Further growth of the particles strongly depends on the properties of the flow into which they are imbedded.

In the current work, a transferred arc is used to produce nanometric particles from the condensation of metallic vapours obtained by controlled evaporation of the anode material, which becomes the solid precursor of the synthesis. As all types of anode materials would be used, depending of the nature of the desired particles, this technique requires a good control of the heat transfer and its application time to a given anode location, as well as the separation of evaporation/ nucleation-growth steps. That is why a new and original experimental set-up was built in order to control vapour production and its thermal history.

Experiments showed that the heat transfer at the anode precursor strongly depends on the cold boundary layer (CBL) properties close to the anode. For adequate parameters, it becomes possible to generate either diffuse or constricted stable arc root, and so to control vapour production. Orientation and so dissociation of evaporation and nucleation events is also achieved by tilting the angle between the jet issued from the cathode and the anode. The vapours produced are then naturally entrained towards a temperature controlled zone, where they are collected onto a water cooled substrate. It thus becomes possible to control the residence time and the thermal vapour history of the particles. Whereas aluminium oxide particles synthesized are clearly nanoparticle chain aggregates, iron oxides particles are spherical, in the micrometric range and no aggregates or agglomerates are visible. These experiments show that particle morphology, size and shape, for given working parameters, strongly depend on the properties of the material to be vaporized.

Keyword: Transferred arc; Nanoparticles; Al_2O_3; Powder-gas phase reaction

1. Introduction

Nanoparticles are considered as fundamental building blocks of nanotechnology. They are the starting point for many 'bottom-up' approaches for preparing nanostructured materials and devices. As such, their synthesis is an important component of rapidly growing research efforts in nanoscale science and engineering. Nanoparticles of a wide range of materials can be prepared by a variety of methods.[1–4]

Gas to particle conversion[5–9] refers to the production of condensed particles from individual atoms or molecules in the gas phase. The particle formation is then driven by the cooling of a supersaturated vapour. The nucleation event is very sensitive to the supersaturation ratio S, defined by the following equation[10]:

$$S = \frac{p_i}{p_S(T)} \tag{1}$$

where p_i is the partial pressure of the gaseous reactant and $p_S(T)$ the corresponding saturated vapour pressure. When this supersaturation ratio becomes larger than unity, nucleation can occur. The critical size d^* for a stable nucleus, which is the size for which the condensation rate balances the evaporation rate, satisfies the following relationship[10,11]:

$$d^* = \frac{4\sigma V}{kT} \ln S \tag{2}$$

* Corresponding author. Tel. +33 5 55 45 75 53: fax: +33 5 55 45 72 11.
E-mail address: jean.jarrige@unilim.fr (J. Jarrige).

0955-2219/$ – see front matter © 2006 Elsevier Ltd. All rights reserved.
doi:10.1016/j.jeurceramsoc.2006.01.018

where V is the monomer volume (m^3), T the temperature (K), σ the surface tension ($N\,m^{-1}$), k the Boltzman constant ($J\,K^{-1}$) and S the supersaturation ratio. Thus, the formation of ultra fine particles occurs only when supersaturation ratios are large. Once particles form in the gas phase, further growth depend on the properties of the flow into with they are imbedded. Therefore, to prepare small particles, it is mandatory to create a high degree of supersaturation, thereby inducing a high nucleation density and then immediately quench the system.

High temperatures and hence high energy sources, such as hydrocarbon flames,[12] laser beam,[13–15] or Joule heating, are often necessary.[16–18] Nevertheless, with such techniques, production rates are poor. Thermal plasma jets produced by dc[19] arcs or RF[20,21] discharges at pressures close to atmospheric pressure are characterized by high temperatures (between 6000 and 14,000 K) of heavy species and medium to high subsonic velocities (between 100 and 2500 $m\,s^{-1}$) of the plasma flow. Ultra fine particles will form in the zone of the plasma reactor where gases have cooled considerably (below 3500 K) and vapours can condense, predominantly via homogenous nucleation.

Thermal plasma based vapour condensation methods utilizing transferred arcs have not been successful up to now to generate fine or ultra fine particles of materials such as metals, alloys, ceramics or composites on a commercial scale because of the poor control of powder properties such as particle size and distribution, shape and crystallinity. For example, Ageorges et al.[22] disclosed the production of ultra fine aluminium nitride particles using a transferred arc with the vapour condensation method. The drawback of their process is due to the fact that the formation of particles occurs in the plasma chamber where are injected the reactive gases. The plasma chamber is "filled with fume products which recirculate in the furnace". As a result, powder properties control is very crude because of the difficulties in proper monitoring of vaporization rate, nucleation and growth of the particles produced within the plasma chamber. To better control the formation of ultra fine aluminium nitride powder, Moura and Munz[23] have proposed the separation of aluminium vaporization and aluminium nitride formation. This is accomplished by vaporizing aluminium anode in a transferred arc reactor in which no reactive gas is introduced, and then reacting the aluminium vapour with ammonia injected at a single point in a separate reactor tube attached to the exit of plasma chamber. It permits better control of powder properties.

The synthesis of ultra fine particles with desired size and composition requires both the control of the partial pressure of reactive precursors and of their thermal history. This requires a good control of the heat transfer to the anode, which depends on properties of the cold boundary layer (CBL) and arc roots dynamic.[24–31] That is why a new experimental set-up was built, allowing controlling vapour production and particle growth kinetics.

2. Experimental set-up

2.1. Presentation

The final objective of this work is to produce nanometric particles from the condensation of metallic vapours obtained by controlled evaporation of the anode material.

A transferred arc reactor was designed (Fig. 1) to generate a stable arc jet, less than 3 mm in diameter, using pure argon, argon–hydrogen mixtures or nitrogen as plasma forming gases (4–10 slm), the power being supplied by a current regulated source (I = 15–40 A). The arc, stabilized by a superimposed plasma jet, is transferred between the cathode made of thoriated tungsten and the anode precursor, made of the material to be eventually proceeded and situated perpendicular to its axis. The pilot arc presents several advantages, such as improving the arc column stability and easing the arc ignition. The pilot arc, first started, feeds with hot ionised gases the gap between the exit nozzle and the anode precursor. Hence, it becomes easier to transfer low current intensity to the anode precursor. The heat flux density transferred to the anode can be regulated with the help of the electrical resistor R (Fig. 1), distributing the current between the stabilization anode-nozzle and the main anode. The experimental set-up developed is adjustable, meaning that it can be rapidly used as well as for ultra fine particles synthesis as for more theoretical studies on arc. For the analysis of plasma properties, the anode is a calorimeter, allowing studying the heat transfer to it and the arc stability.

For nanoparticles synthesis, the anode is made of the material to be vaporised (aluminium, iron, copper, ...). Besides the target is rotating, permitting the temperature control at the

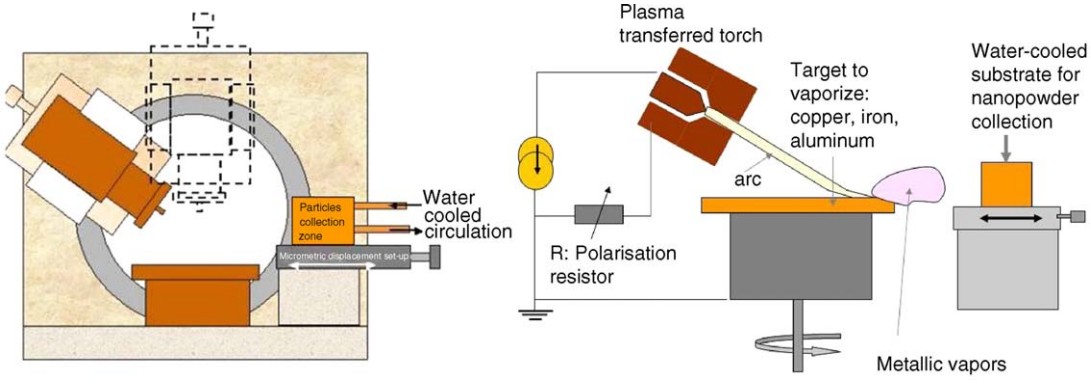

Fig. 1. Experimental set-up developed.

arc attachment, and thus, the vaporization flux. Furthermore, the pilot arc allows rising the plasma jet momentum, permitting its inclination. As the torch assembly is mounted on "ball bearings", the angle between the jet axis and the normal to the anode surface can be changed continuously from $\theta = 0$ to 85°, whereas the electrode gap can vary from 1 to 25 mm. Beyond the modification of the heat transfer mechanisms, this inclination allows orientating the metallic vapours toward a pressure and temperature controlled zone. Hence, the control of vapour thermal history becomes possible.[22,23]

2.2. Submicronic or nanometric particles analysis

Microstructural features of particles produced were studied using the scanning electron microscopy (SEM) (Philips XL 30). If the particles synthesised were too small to be visualised by SEM, the collected powder was dispersed ultrasonically in alcohol and then disposed on carbon coated copper grids for investigation by a transmission electron microscopy (TEM JEOL 2010). The chemical composition of the particles was obtained from XRD diagrams. The diffraction pattern of the powder was recorded at a speed of 0.04° s^{-1} using Cu Kα radiation.

3. Results and discussion

3.1. Heat flux to the anode

Heat power transferred to the anode material comes from two different contributions. The first one is due to convective heat transfer between the plasma flow and the anode wall, and the other one is due to the energy released by electrons entering the metal. This last part gives an electronic contribution to the total power which is given by[32]:

$$P_{\text{elec}} = I\left(\frac{5}{2}kT_{\text{e}} + W_{\text{s}} + V_{\text{a}}\right) \tag{3}$$

where I is the arc current, T_{e} the electron temperature, V_{a} the anodic fall and W_{s} the work function of the anode material. In situations encountered in this work, the above parenthesis represents a total value comprised between 10 and 15 V.

The heat flux due to electron is concentrated over a rather tiny area, in contrast with the convective contribution which is spread over a wider surface. The P_{elec} contribution is located at the anode arc attachment, and gives the flux:

$$\varphi_{\text{elec}} = \frac{4\,P_{\text{elec}}}{\pi\,d_{\text{s}}^2} \tag{4}$$

where d_{s} is the diameter of attachment area.

The arc attachment is diffused when controlled by the plasma jet momentum or, at the opposite, is constricted when dominated by self induced magnetic forces. Depending of the attachment mode, which determines the d_{s} value, the φ_{elec} value can be changed over about an order of magnitude, ranging typically from a few 10^7–10^9 W m^{-2}, for a given P_{elec} value compatible with the operating parameters.

3.2. Anode temperature control

The anode material must be evaporated slowly and continuously, in order to have a regular production of vapour. The heat flux must be supplied in the constricted attachment mode to reach a sufficiently high level, but, in the same time, must be adjusted to avoid the cutting of the anode, or a to high ejection rate of melted droplets.

The anode is rotated at a given angular speed, ω, so that the time of stagnation of a given point of the surface is approximately:

$$t_{\text{s}} = \frac{d_{\text{s}}}{\omega\ell} \tag{5}$$

where ℓ is the distance between the rotation axis and the thermal impact at the anode surface. The anode is mounted onto a water cooled holder, so that the bulk mean temperature of the material remains approximately constant. Due to the rotative motion, each point at the surface approaching the area where the arc impinges is submitted to a transient heat flux, which gives the following temperature rise[33]:

$$T(t) = T_w + \frac{2\varphi_{\text{el}}}{\kappa}\sqrt{\frac{\alpha t}{\pi}} \tag{6}$$

where T_w is the temperature of the anode surface before thermal treatment begins, and κ and α are respectively the thermal conductivity (W/m K) and thermal diffusivity ($m^2\ s^{-1}$) of the anode material. The melting temperature, T_{m}, is thus reached within a

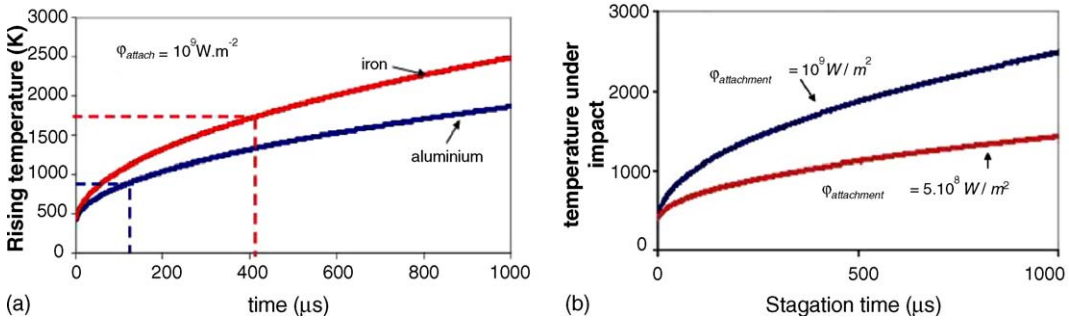

Fig. 2. Effect of anode material properties (a) and heat flux density (b) on temperature rise under arc root attachment.

time, t_m, so that:

$$t_m = \frac{\pi}{\alpha}\left[\frac{k(T_m - T_w)}{2\varphi_{el}}\right]^2 \quad (7)$$

A good compromise for the experimental parameters is to set $t_s \approx t_m$, by adjusting the rotation speed $\omega$for a given material and a given arc current.

It must be underlined that following Eqs. (4) and (7), t_m is strongly depending upon the spot size d_s and so φ_{elec}. Fig. 2a illustrates the effect of anode material (aluminium or iron), for a given heat flux and Fig. 2b the effect of the heat flux, for an iron anode precursor.

It can be noted that the iron target temperature rises faster than that of the aluminium one. This is due to the higher diffusivity of aluminium compared to that of iron (see Table 1). Nevertheless if it is supposed that vapour production is high enough when the melting temperature is reached, it becomes obvious that the thermal diffusivity of the material is a key parameter. Effectively, for a given heat flux, 10^9 W/m^2, it takes 200 μs to reach the melting temperature for an aluminium anode, whereas approximately 400 μs are needed for iron.

Fig. 2b clearly illustrates the strong influence of the heat flux on vapour level production. As well, both the control of the heat flux and its application time are necessary for monitoring reactive species production. Thus, in order to control the vapour production, the anode precursor is disposed at the top of a rotating substrate permitting the temperature control at the arc attachment, and thus, the vaporization flux. Thus, for given heat flux and rotating speed, different tracks allow controlling the application time of the heat flux transferred. However, it must be inferred that a too high rotating speed would favour arc root attachment instabilities,[34] leading to a very poor control of the partial pressure as well as the residence time of the reactive species, as illustrated in the following section.

Table 1
Thermal properties of the anode precursor

	Thermal diffusivity (m^2 s^{-1})	Melting temperature (°C)
Aluminium	2.2×10^{-4}	1538
Iron	10^{-3}	660

3.3. Attachment stability

The synthesis of desired particles requires both the control of the heat flux transferred to the anode and the plasma flow characteristics which determine the imbedded metallic vapour kinetics. The first step of this work consisted in determining the heat flux transferred to the anode surface in order to control the partial pressure of reactive species. The second part of the study deals with the effect of the orientation of the generated vapours, performed by tilting the angle between the plasma jet and the normal to the anode surface. It allows controlling the residence time of the particles before collection.

The constricted attachment is obtained when the magnetic forces overcome those induced by the normal component of the jet momentum. This situation can be obtained by tilting the plasma jet, but, in the same time, the tangential component may lead to the sliding motion of the arc root. The arc attachment becomes unstable and jumps from place to place at the anode surface. As the tilting angle rises from 0° to almost 90°, (fully tangential), three different kinds of attachment can be distinguished: the diffused and stable mode, the constricted and stable mode and finally the constricted unsteady mode (see Fig. 3).

As shown in a previous work,[35] tilting progressively the torch relatively to the substrate normal induces different behaviours of the arc root.

Below a tilting angle of about 55° (see Fig. 3a and b) for argon–hydrogen (75/25 vol%) the arc root seems to be diffused and the cold boundary layer thickness between the arc and the

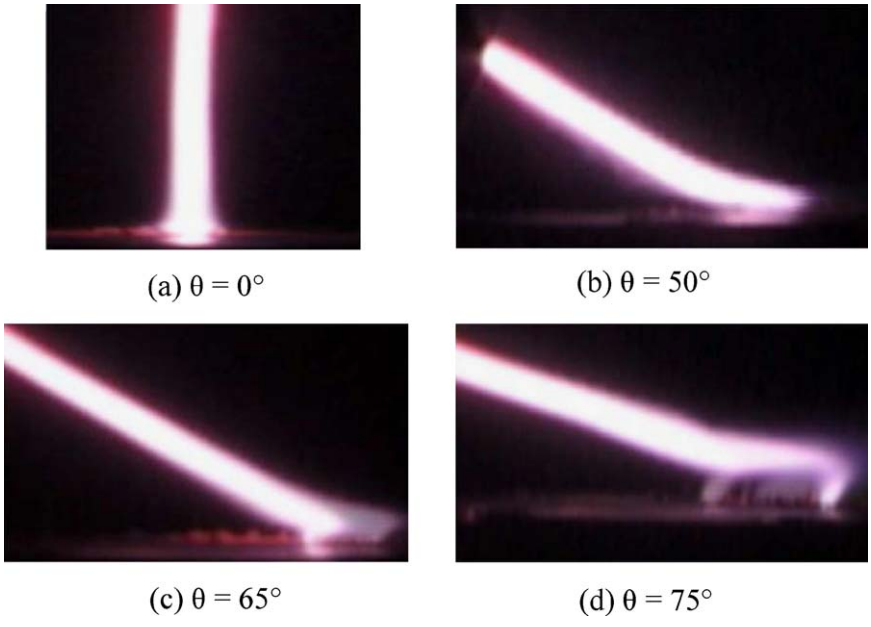

Fig. 3. Arc root attachment dynamic and geometry as a function of the tilting angle: Ar–H_2 (75–25 vol%), $I = 20$ A, electrode gap $d_{a-k} = 21$ mm.

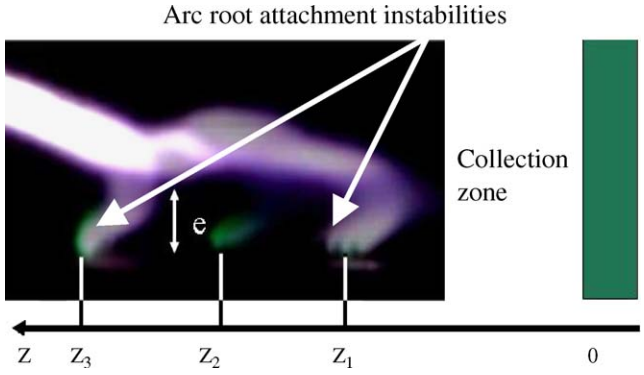

Fig. 4. Effect of arc root instabilities on residence time of particles.

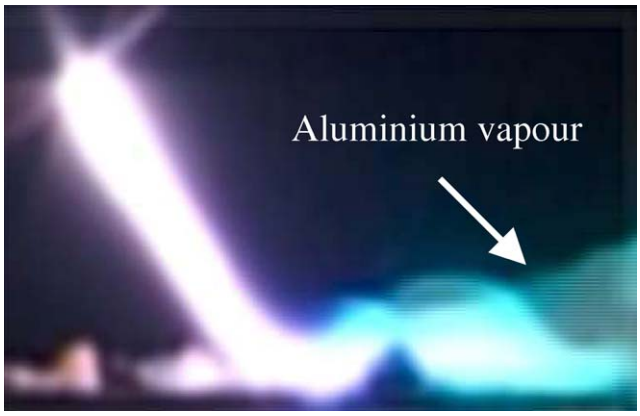

Fig. 5. Stable and constricted arc root on an aluminium anode precursor.

anode, e, is thin (below a few tenth of micrometers), corresponding to a cathode jet dominated mode.[25] The diffuse attachment mode is not very useful for particle production because the vaporized material is confined close to the anode by the cathode jet and its escape in the anode attachment fringes is not controlled at all. Moreover, the quantity produced is low because the heat flux at the anode is low.

Over these angle values, the cold boundary layer thickness increases drastically with the tilting angle. The arc root becomes strongly constricted at the anode (see Fig. 3c) with a stable attachment below about 65° and strongly unstable afterwards (see Fig. 3d). In the case of an unstable attachment (see Figs. 3d and 4), the arc column is stretched by the flow acting on the arc-anode connexion, this movement being accompanied by an increase of the arc voltage and of the electric field in the sheath. Once the field in the sheath is high enough to induce an electrical breakdown, a new attachment is initiated, and simultaneously, the previous one extinguishes (Fig. 3d). These instabilities are damageable because vapour production can't any more be controlled. Furthermore, the residence time, for a given collection distance, would be drastically modified by these instabilities. Effectively, even if it is supposed that reactive species production is not affected by these instabilities, it is easy to understand that the residence time, for fixed collection zone, will be increased if vapours are produced at z_3 (see Fig. 4) instead of z_1. They would favour synthesis of particles with different sizes and compositions, resulting in poor reproducibility. In the case of a stable and constricted attachment, the vaporized material is entrained in a rather well defined direction and its residence time and/or reaction with the surrounding atmosphere can be controlled (see Fig. 5).

As the arc current intensity and plasma forming gas condition the nature of the particles to be produced, it could be interesting, for given working parameters, to visualise their effects on the arc root attachment properties. The main result is that adding hydrogen delays the shifting from one mode to another. That can be explained by the fact that shifting from argon to argon hydrogen as plasma forming gas results into a better heat transfer and a higher jet velocity. Hence, the cold boundary layer is longer governed by mechanical effect and higher angles are needed to shift from one mode to another. Same results are obtained when increasing arc current or decreasing the nozzle internal diameter of the arc pilot. So, as the key-point of this process consists in keeping the heat flux density at a critical value for which anode erosion is only due to its vaporization, minimizing droplet ejection, the torch tilting must be set-up in order to obtain a constricted and stable arc root attachment, as in Fig. 5. A stable and constricted arc root allows both the reproducibility of synthesis and vapour phase production control, and also enhances by about one order of magnitude the heat flux transferred to the anode precursor.

3.4. Particle synthesis

Experiments presented here were performed at atmospheric pressure, in air. Thus, the control of the chemical composition was not possible and mainly oxides were formed. In order to illustrate the influence of the anode precursor material on particle properties, aluminium and iron, were successively treated for given working parameters.

3.4.1. Aluminium particles

The experimental parameters are summarised in Table 2.

Working parameters were chosen in order to properly vaporize the aluminium target, with almost no melting. With such parameters, the arc root is constricted and stable (Fig. 5). Due to the high power level transferred to the anode precursor, vaporisation of anode precursor occurs. The vapours are naturally canalised by the plasma flow towards the collecting substrate. The particles are collected onto a water-cooled substrate, mounted on a micrometric displacement set-up (see Fig. 1 right)

Table 2
Working parameters for alumina and iron oxides synthesis

Plasma gas	Ar
Intensity transferred (A)	15
Total voltage (V)	50
Gas flow rate (L/min)	4
Angle (°)	45
Nozzle internal diameter (mm)	2.5
Collection distance (mm)	20
Rotating speed (cm s^{-1})	0.5

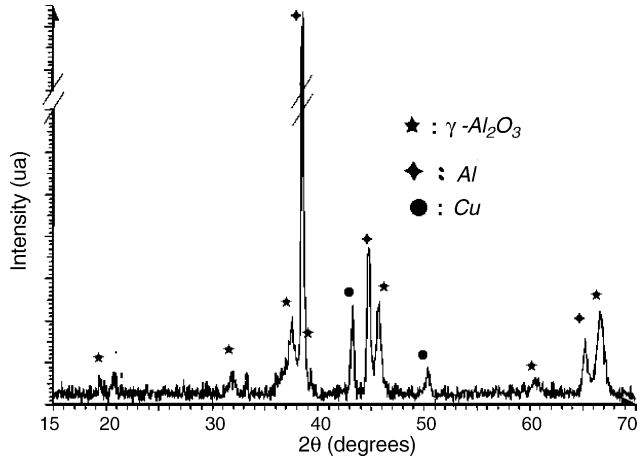

Fig. 6. XRD diagrams: aluminium (AU 4G) as anode precursor.

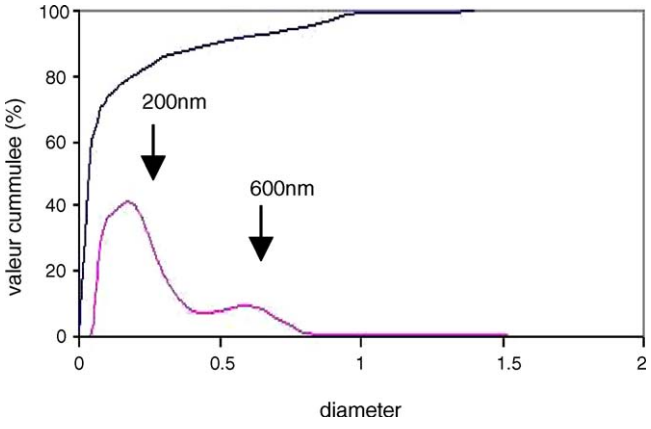

Fig. 7. Particle size distribution obtained by laser scattering method.

in order to modify the residence time of particles imbedded in the flow.

X-rays diffraction results (Fig. 6) of the collected powder indicate that it is heterogeneous, comprising γ Al_2O_3 and not yet reacted Aluminium. As no oxygen quenching of the plasma plume was performed during experiments, the formation of oxides can be explained as follows. For appropriate working parameters, vaporization of metallic precursor occurs. These vapours are naturally canalised by the plasma flow towards the water cooled substrate for collection. Nevertheless, due to viscous strength, air is entrained in the fringes of the plasma jet and diffuses inside its core, where O_2 is dissociated. The entrained oxygen and its dissociation as well as the jet expansion and probably also, to a lesser extend, the water cooled surface cool down the plasma jet with its aluminium vapour, resulting in the nucleation of solid aluminium as well as γAl_2O_3. The latter corresponds probably to the gas phase reaction of aluminium and atomic oxygen. Unfortunately, the quantity of oxygen entrained being uncontrolled, only part of the aluminium nanoparticles are oxidized. For the aluminium target, the presence of copper can be explained by the fact that the aluminium precursor comprised 4 wt% copper. The presence of broadened peaks from normal X-ray patterns, proves that the particles are not completely crystallized and in the nanometric range (below 100 nm). The formation of alumina gamma phase, in preference to the thermodynamically stable α phase, is consistent with the highly non equilibrium nature of the process. Vapours of aluminium react with oxygen to form aluminium oxide, which crystallizes in the metastable γ phase by virtue of the rapid quench associated with the process.

Particle size distribution of the processed powder is shown in Fig. 7. It is obvious that all the particles are in the submicrometer range. That can be explained by the very good control of the vaporization process, avoiding droplet ejection, and by the dissociation of the vaporization and nucleation/growth events. By the way, it must be underlined that the reproducibility of the experiments is achieved. Two main peaks can be distinguished, one centred on 200 nm and the other on 600 nm. As ultra fine particles have an inherent tendency to form agglomerates and aggregates, the results of particle size distribution studies by laser scattering mostly give the size distribution of these agglomerates. The actual size of the individual particles in the clusters can be determined by scanning and transmission electron microscopy. The micrographs obtained are presented in Figs. 8–10.

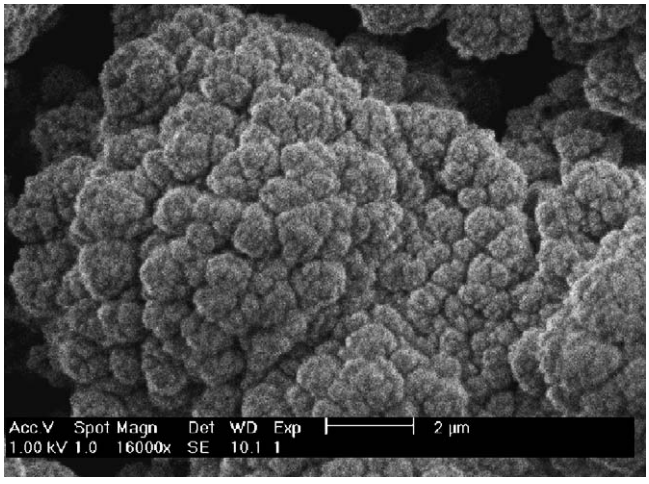

Fig. 8. SEM observation of the particles synthesised with aluminium as anode material.

SEM results (Fig. 8) tend to prove that the particles are of the cauli-flower type. These agglomerates, which are in

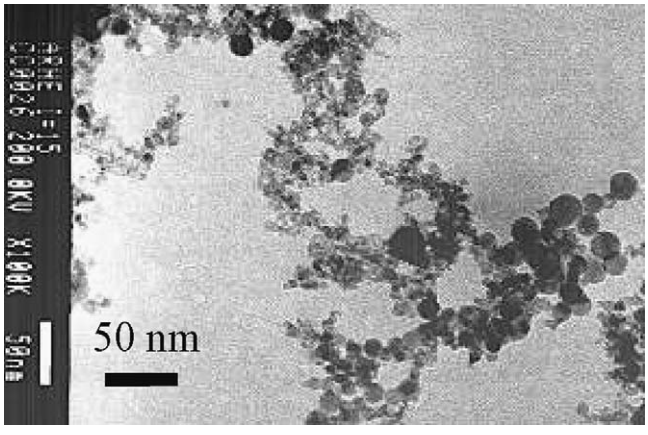

Fig. 9. TEM observation of the alumina and aluminium powder.

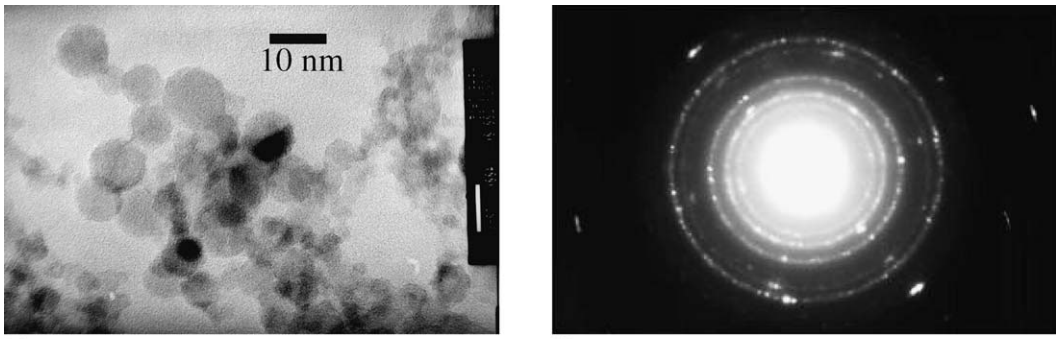

(a) (b)

Fig. 10. TEM observation of the alumina powder (a) and associated XRD diagram (b).

the submicronic range, and are easily separated by ultrasonic dispersion in alcohol (no big aggregates) are composed of nanosized particles, as shown in Figs. 9 and 10. The discontinuous rings (Fig. 10b) of the XRD diagram associated with the TEM observation of Fig. 10a confirms that particles are nanosized. The TEM observation also confirms that ultra fine particles have tendency to form agglomerates.

The spherical or near spherical morphology of the powder is obvious (see Fig. 10a), but they tend to form small agglomerates, whose compactness depends of ramifications orientation. The aggregates are resolved into individual particles with size ranging from a few nanometers to about 40 nm. Aggregates are formed by sintering of primary particles during the synthesis process. These aggregates often have a fractal-like, highly branched structure and reach a size of about 300 nm in several dimensions. In some applications, such as catalysis, agglomerates with an open structure like those are desired. However, in many potential applications nonagglomerated spherical nanoparticles of uniform size are needed. X-ray diagram (Fig. 10b) proves that particles are well crystallized, even if some are not.

It could be interesting to visualize the effect of the residence time, in order to determine if it is possible to control the morphology and/or the composition of the particles. The residence time of the vapour imbedded in the plasma jet may be an important parameter for particle properties. This time must be defined as the time which is passed by between the moment where nucleation occurred and particles are collected. As it is quasi impossible to define precisely the location where vapour nucleates, it is nevertheless possible to increase and control the residence time by moving back the water cooled substrate onto which particles are collected. Viability of such an experiment involves a stable arc root attachment, in order to maintain the same evaporation flux and the same nucleation location. Hence, by moving back the substrate, residence time can be increased.

The pictures in Fig. 11 correspond to particles obtained from an aluminium target. The working parameters are those presented in Table 2, but collecting substrate was moved back of 10 mm between Fig. 11a and b. From the TEM pictures, no real distinction and differences can be established. The particles are in both cases nanosized, aggregated with an open structure. Depending of the orientation of the ramifications, the aggregates could become more compact, which could lead to bigger particles. By the way, X-ray diffraction pattern obtained for case (b) shows that the composition is identical but peaks are thinner. This could mean that the powder is either better crystallized or bigger.

3.4.2. Iron oxide particles

Another key parameter is the nature of the powder to synthesize, which is set by the chemical composition of the target to be vaporized. In order to illustrate the effects of the anode material on particle properties, an iron target was vaporised with the same working parameters, as those presented in Table 2. Compared

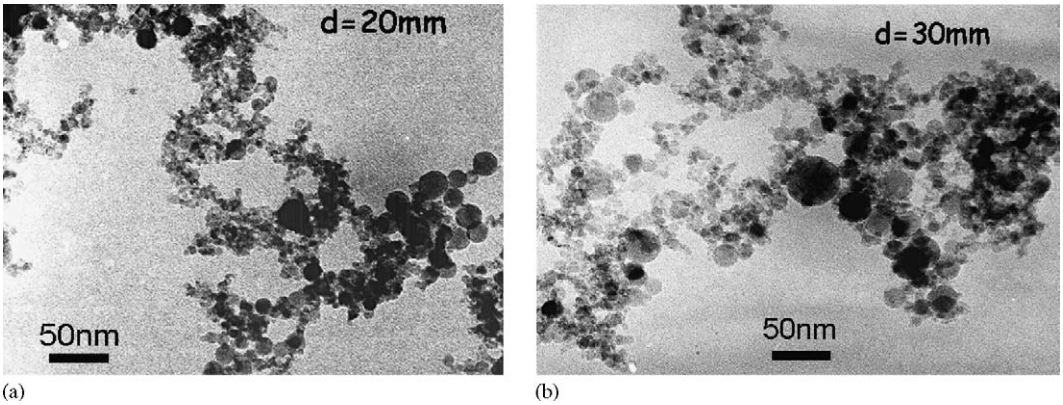

(a) (b)

Fig. 11. TEM pictures of alumina particles: effect of residence time on size and morphology.

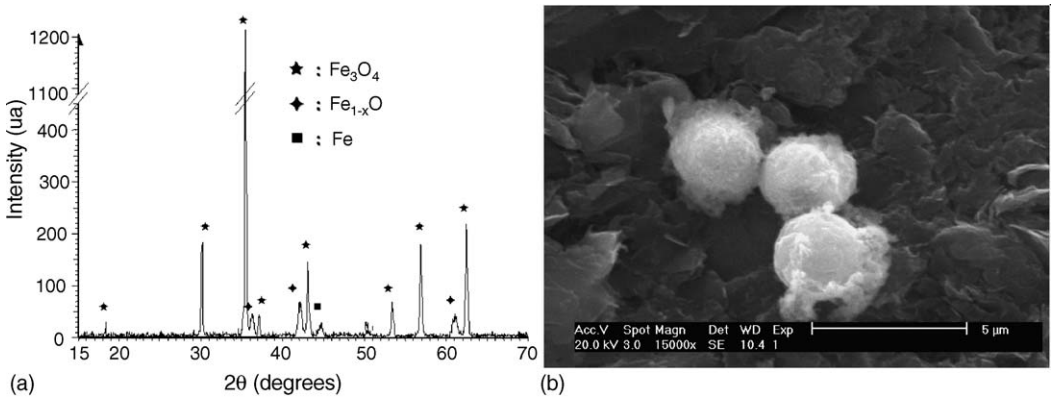

Fig. 12. X-rays pattern of the powder obtained. (a) Iron as anode material, $I = 15$ A, d_{a-k}=12mm, Ar = 5 L/min, exit nozzle i.d = 2.5 mm and (b) iron as anode precursor.

to aluminium, iron presents higher melting temperature, lower volatility and thermal diffusivity (Table 1).

Starting from the iron target, Fig. 12a shows that main crystallised phases synthesized are magnetic iron oxide Fe_3O_4, but also FeO and Fe can be found, showing that oxygen is the limiting species. Formation of oxides is again explained by the air which is entrained from the fringes of the plasma and diffuses towards its core, where O_2 is dissociated. Hence, atomic oxygen can react with atomic metallic vapour to form oxides. The thin peaks tend to prove that particles are not nanosized.

SEM micrograph in Fig. 12b is a typical sample of particles produced with an iron target and confirms that they are in the micrometric range and spherical. No aggregates or agglomerates are visible. Hence, this experiment shows that particle morphology, size and shape, for given working parameters, strongly depend of the properties of material to be vaporized. No real explanation can be proposed, due to the very complex phenomena occurring during nucleation and growth. Nevertheless, it could be noticed that for this given parameters, which are set to properly vaporize aluminium, iron vapour production was not properly controlled, resulting in the ejection of liquid droplets and solid fragments. Furthermore, with such working parameters, the vapour phase production was very low. This could explain the spherical morphology as well as the micrometric ranging size of the particles, which are not, in that case, synthesized from the gas to particle conversion route.

4. Conclusion

Gas to particle conversion refers to production of particles from individual atoms or molecules in the gas phase. In the current work, the anode of the transferred arc is considered as the solid precursor of the synthesis. The process consists in keeping the local heat flux at a critical value for which anode erosion is only due to its vaporization. As powder with controlled size and composition requires the dissociation of the vaporization and nucleation event, a new experimental set-up has been developed. The first step of the synthesis has consisted in studying the heat transfer to the anode precursor as a function of transferred arc operating parameters, while the second consists in controlling, for a given heat flux, the rise of temperature under the arc attachment. These experiments clearly show the influence of the anode material on particle properties. Orientation and so dissociation of nucleation event is achieved by tilting in a given range the angle between the plasma column and the normal to the anode-substrate. The transferred arc is controlled by a blown arc and the tilting angle range is chosen to achieve a stable and constricted arc root attachment, generating an anode jet in a well controlled direction. The vapours produced are naturally entrained and orientated towards a temperature controlled zone, where they are collected onto a water cooled substrate. The particles synthesised result from the metal vapour reaction with the oxygen of the entrained air. Their composition is heterogeneous (alumina and aluminium, because oxygen is the limiting reactive species. For an aluminium anode, results of X-ray diffraction of the powder produced shows that the particles are nanosized and mainly crystallized under the gamma phase for the alumina. Aluminium oxides particles synthesized are clearly nanoparticle chain aggregates initially about few hundred nm long, composed of primary particles that are approximately 10 nm, even if particles with diameters reaching 40 nm can be observed. In some applications, such as catalysis, agglomerates with an open structure like those are desired. However, in many potential applications nonagglomerated spherical nanoparticles of uniform size are needed. For fixed transferred arc operating parameters, particles obtained from an iron target are completely different. They are mainly spherical, not nanosized (a few micrometers) and no aggregates or agglomerates are visible. Due to the very complex phenomena occurring during nucleation and growth no real explanation can be proposed. Nevertheless, it could be noticed that for these given parameters, which were set to properly vaporize aluminium, iron vapour production wasn't properly controlled, resulting in liquid droplets and solid fragments ejection. This could explain the spherical morphology as well as the micrometric ranging size of the particles, which are not, in that case, synthesized from the gas to particle conversion route. These experiments show that particle morphology, size and shape, for given working parameters, strongly depend on the properties of material to be vaporized and the adaptation of the transferred arc parameters to them.

Nevertheless the most important result is probably the fact that the reproducibility of the experiment is achieved. More experimental studies are needed using a wider range of materials and operating conditions, with well-controlled geometries and flow regimes.

Acknowledgement

Authors would like to thanks Dr. Grimaud, engineer at the University of Sciences and Technology of Limoges, for his technical knowledges, advices and attention. Without him, this work could not have been performed.

References

1. Yongqing, Z., Zihua, Y., Shiwen, D., Mande, Q. and Jian, Z., Synthesis and characterization of Y_2O_3:Eu nanopowder via EDTA complexing sol–gel process. *Mater. Lett.*, 2003, **57**(19), 2901–2990.
2. He, Y.-Q. and Ping, Y.-H., Nano-composite TiO_2–PI via sol–gel process. *Mater. Chem. Phys.*, 2003, **78**(3), 614–619.
3. Lam, C., Zhang, Y. F., Tang, Y. H., Lee, C. S., Bello, I. and Lee, S. T., Large-scale synthesis of ultrafine Si nanoparticles by ball milling. *J. Cryst. Growth*, 2000, **220**(4), 466–470.
4. Zhang, Q. and Saito, F., Mechanochemical synthesis of $LaMnO_3$ from La_2O_3 and Mn_2O_3 powders. *J. Alloys Compd.*, 2000, **297**(2), 99–103.
5. Zachariah, M. R., Carrier, M. J. and Blaisten-Barojas, E., Properties of silicon nanoparticles: a molecular dynamics Study. *J. Phys. Chem.*, 1996, **100**, 14856–14864.
6. Zachariah, M. R., Shull, R. D., McMillin, B. K. and Biswas, P., In situ characterization and modeling of the vapour phase growth of a supermagnetic nanocomposite. *Nanotechnology*, 1996, **622**(3), 42–63.
7. Hahn, H., Gas phase synthesis of nanocrystalline materials. *Nanostruct. Mater.*, 1997, **9**, 3–12.
8. Kruis, F. E., Fissan, H. and Peled, A., Synthesis of nanoparticles in the gas phase for electronic, optical and magnetic applications—a review. *J. Aerosol. Sci.*, 1998, **29**, 511–535.
9. Morjan, I. *et al.*, Carbon nanopowders from the continuous-wave CO_2 laser-induced pyrolysis of ethylene. *Carbon*, 2003, **41**(15), 2913–2921.
10. Friedlander, S. K., Dynamics of aerosol formation by chemical reaction. *Ann. N. Y. Acad. Sci.*, 1983, **404**, 354–364.
11. Girshick, S. L. and Chiu, C. P., *Plasma Chem. Plasma Process.*, 1989, **9**, 355–365.
12. Madler, L., Kammler, H. K., Mueller, R. and Pratsinis, S. E., Controlled synthesis of nanostructured particles by flame spray. *J. Aerosol. Sci.*, 2002, **33**(2), 369–389.
13. Martelli, S. *et al.*, Production of iron-oxide nanoparticles by laser-induced pyrolysis of gaseous precursors. *Appl. Surf. Sci.*, 2000, **154-155**, 353–359.
14. Morjan, I., Alexandrescu, R., Soare, I., Dumitrache, F., Sandu, I., Voicu, I. *et al.*, Nanoscale powders of different iron oxide phases prepared by continuous laser irradiation of iron pentacarbonyl-containing gas precursors. *Mater. Sci. Eng. C*, 2003, **23**(1-2), 211–216.
15. Yang, X. C., Riehemann, W., Dubiel, M. and Hofmeister, H., Nanoscaled ceramic powders produced by laser ablation. *Mater. Sci. Eng. B*, 2002, **95**(3), 299–307.
16. Pratsinis, S. E. and Kodas, T. T., In *Manufacturing of Materials by Aerosol Processes in Aerosol Measurement*, ed. K. Willeke and P. Baron. Van Nostrand Reinhold, New York, 1993, pp. 721–746, Chapter 33.
17. Granquist et Buhrman, Ultrafine metal particles. *J. Appl. Phys.*, 1976, **47**(5), 2200–2219.
18. Adjaottor and Griffin, Aerosol Synthesis of Aluminum Nitride Powder Using Metalorganic Reactants. *J. Am. Ceram. Soc.*, 1992, **75**, 3209–3214.
19. Oh, S. M. *et al.*, Production of ultrafine titanium dioxide by DC plasma jet. *Thin Solid Films*, 2001, **386**(2), 233–238.
20. Viera, G., García-Caurel, E., Costa, J., Andújar, J. L. and Bertran, E., Nanoparticles of Si–C–N from low temperature RF plasmas: selective size, composition and structure. *App. Surf. Sci.*, 1999, **144-145**, 702–707.
21. Sugasawa, M., Kikukawa, N., Ishikawa, N., Kayano, N. and Kimura, T., Synthesis of Y–Fe–O ultrafine particles using inductively coupled plasma. *J.Aeroso. Sci.*, 1998, **29**(5–6), 675–686.
22. Ageorges, H., Megy, S., Chang, K., Baronnet, J. M., Williams, J. K. and Chapman, C., Synthesis of aluminium nitride in transferred arc plasma furnaces. *Plasma Chem. Plasma Process.*, 1993, **13**(4), 613–632.
23. Moura, J. F. and Munz, J. R., Vapor-phase synthesis of nanosize aluminum nitride particles using a two-stage transferred arc reactor. *J. Am. Soc.*, 1997, **80**(9), 2425–2428.
24. Sanders, N. and Pfender, E., Measurement of anode falls and anode heat transfer in atmospheric pressure high intensity arcs. *J. Appl. Phys.*, 1984, **55**(3), 714–722.
25. Dinulescu, H. A. and Pfender, E., Analysis of the anode boundary layer of high intensity arcs. *J. Appl. Phys.*, 1980, **51**(6), 3149–3157.
26. Leveroni, E. and Pfender, E., In *Proceedings of the 9th International Symposium on Plasma Chemistry (Pugnochiuso), Vol* **1**, ed. R. d'Agestino, 1989, pp. 336–365.
27. Jenista, J. and Heberlein, J., Numerical model of the anode region of high-current electric arcs. *IEEE Trans. Plasma Sci.*, 1997, **25**(5), 883–890.
28. Amakawa, T., Jenista, J., Heberlein, J. and Pfender, E., Anode boundary layer behaviour in a transferred high intensity arc. *J. Phys D: Appl. Phys.*, 1998, **31**, 2826–2834.
29. Mehmetoglu, M. T. and Gauvin, W. H., Characteristics of transferred arc plasma. *AIChE J.*, 1983, **29**, 207–215.
30. Sanders, N., Etemadi, K., Hsu, K. C. and Pfender, E., Studies of the anode region of a high intensity argon arc. *J. Appl. Phys.*, 1982, **53**(6), 4136–4145.
31. Girshick, S. L., Li, C., Yu, B. W. and Han, H., Fluid boundary layer effects in atmospheric-pressure plasma diamond film deposition. *Plasma Chem. Plasma Process.*, 1993, **13**(2), 169–187.
32. Pfender, E., In *Proceedings of the Julian Szekely Memorial Symposium on Materials Processing*, ed. H. Y. Sohn, J. W. Evans and D. Apelian. TMS Publication, 1997, pp. 475–502.
33. Carlsaw, S. and Jaeger, J. C., *Conduction of Heat in Solids* (*2nd ed.*). Oxford University Press, Amen House, London, 1959, E.C.4, pp. 263–265.
34. Sobrino, J. M., Coudert, J. F. and Fauchais, P, In *Proceedings of the 12th ISPC, Minneapolis, Vol* **3**, ed. J. Heberlein, 1995, pp. 1455–1460.
35. Chazelas, C., Coudert, J. F. and Fauchais, P., Arc root behaviour in a plasma spray torch. *IEEE Trans. Plast. Sci.*, 2005, **33**(2), 416.